# Large Exciton Energy Shifts by Reversible Surface Exchange in 2D II–VI Nanocrystals

Yang Zhou, Fudong Wang, and William E. Buhro*

Department of Chemistry, Washington University, Saint Louis, Missouri 63130-4899, United States

S *Supporting Information*

ABSTRACT: Reaction of *n*-octylamine-passivated {CdSe[*n*-octylamine]$_{0.53\pm0.06}$} quantum belts with anhydrous metal carboxylates M(oleate)$_2$ (M = Cd, Zn) results in a rapid exchange of the L-type amine passivation for Z-type M(oleate)$_2$ passivation. The cadmium-carboxylate derivative is determined to have the composition {CdSe[Cd(oleate)$_2$]$_{0.19\pm0.02}$}. The morphologies and crystal structures of the quantum belts are largely unaffected by the exchange processes. Addition of *n*-octylamine or oleylamine to the M(oleate)$_2$-passivated quantum belts removes M(oleate)$_2$ and restores the L-type amine passivation. Analogous, reversible surface exchanges are also demonstrated for CdS quantum platelets. The absorption and emission spectra of the quantum belts and platelets are reversibly shifted to lower energy by M(oleate)$_2$ passivation vs amine passivation. The largest shift of 140 meV is observed for the Cd(oleate)$_2$-passivated CdSe quantum belts. These shifts are attributed entirely to changes in the strain states in the Zn(oleate)$_2$-passivated nanocrystals, whereas changes in strain states and confinement dimensions contribute roughly equally to the shifts in the Cd(oleate)$_2$-passivated nanocrystals. Addition of Cd(oleate)$_2$, which electronically couples to the nanocrystal lattices, increases the effective thickness of the belts and platelets by approximately a half of a monolayer, thus increasing the confinement dimension.
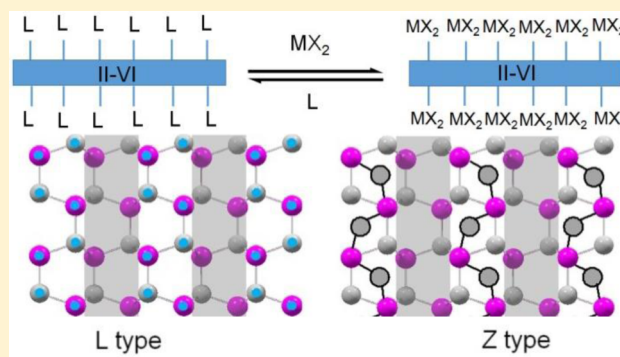
INTRODUCTION

We now report that surface exchange between amine-passivated (L-type)[1] and metal-carboxylate-passivated (M = Cd, Zn; Z-type[1]) surfaces of CdSe and CdS quantum belts (QBs, nanoribbons) and platelets (QPs) induces exciton energy shifts as large as 140 meV in the extinction (absorption) and emission spectra. These shifts and the nature of the surface passivation are fully reversible. The reversible electronic perturbations are attributed to changes in the strain states and confinement dimensions of the 2D nanocrystals upon surface exchange. We propose the surface passivation effects to be magnified in the 2D nanocrystals relative to semiconductor nanocrystals of other morphologies because of their very large surface fractions and thin confinement dimension.

Exchange of the surface passivation in semiconductor nanocrystals often profoundly influences photoluminescence efficiencies,[2−4] but it generally does not induce significant energetic shifts in their absorption and emission features. For example, Owen and co-workers recently reported that the surface passivation of CdSe (and other) pseudospherical nanocrystals (quantum dots) may be reversibly exchanged between neutral-acceptor (Z-type) Cd(carboxylate)$_2$ passivation and neutral-donor amine passivation (Scheme 1).[1] Although the exchange produces large effects on nanocrystal photoluminescence quantum yields, the lowest-energy absorption feature shifts by only ∼4 meV (a ∼1 nm shift of a 565 nm

Scheme 1. Exchange of Z- and L-Type Surface Passivation in II–VI Quantum Dots[1]
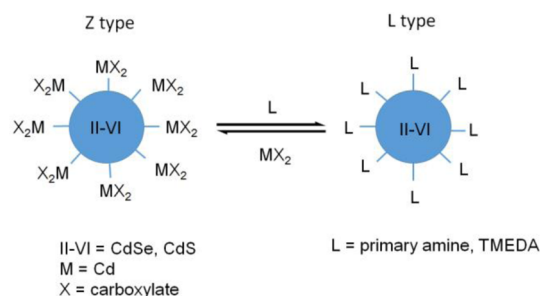
absorbance).[1] Large shifts in the absorption spectra of semiconductor nanocrystals upon changes in surface ligation are not typically observed.

A few counterexamples to the rule above have been described. Weiss and co-workers demonstrated that the incorporation of phenyldithiocarbamate (PTC) ligands onto the surfaces of II–VI and IV–VI nanocrystals may result in shifts of the lowest-energy absorption feature of up to 1 eV to lower energy.[5] In these systems, holes delocalize into the PTC ligand shells, increasing the effective confinement dimension

(that is, increasing the box size) and thus decreasing the confinement potential. Thiol, selenol, or tellurol ligation is observed to have a similar effect in II−VI nanocrystals, but it is smaller in magnitude (energy shifts of 10−40 meV).[6−8] In these latter cases, electronic coupling between the nanocrystal and ligand shell apparently extends the crystal lattice and increases the size of the confinement box.

Lattice strain also modifies the effective band gaps of semiconductor nanocrystals.[9−14] Compressive strain decreases bond distances in nanocrystals, thus increasing orbital overlap and effective band gaps, which shifts absorption and emission features to higher energies.[13] Tensile strain induces the opposite effects: longer bond distances, decreased orbital overlap, decreased effective band gaps, and spectral shifts to lower energies. The strain states of semiconductor nanocrystals are significantly influenced by surface passivation and the nature of the resulting surface reconstructions.[15−17] For example, colloidal CdSe quantum dots passivated by hexadecylamine experience a compressive surface reconstruction, whereas those passivated by TOPO experience a tensile surface reconstruction.[17] In 2D II−VI nanocrystals, compressive and tensile strains as large as 6 and 8%, respectively, have been observed as functions of both passivation and core crystal structure.[18,19]

Herein, we elucidate the contributions of lattice strain and confinement dimension to the effective band gap changes in 2D CdSe and CdS nanocrystals upon exchange between L- and Z-type surface passivation (Scheme 2). We show that the

Scheme 2. Exchange of Z- and L-Type Surface Passivation in 2D II−VI Nanocrystals
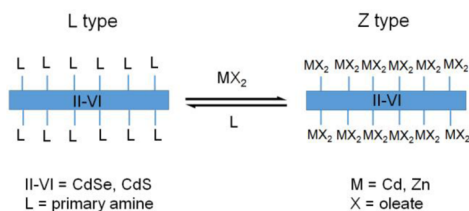
reversible shifts in the absorption spectra between L- and Z-type passivation have roughly equal contributions from changes in strain and dimensionality with $Cd(oleate)_2$ as the Z-type passivation. The smaller reversible shifts observed with $Zn(oleate)_2$ as the Z-type passivation are due entirely to changes in the strain states of the nanocrystals. The results establish that the $Cd(oleate)_2$ passivation couples to the electronic structure of the nanocrystal core, increasing the confinement dimension (box size), whereas, as expected, the $Zn(oleate)_2$ passivation does not.

■ EXPERIMENTAL SECTION

Materials and General Procedures. Cadmium acetate dihydrate ($Cd(OAc)_2 \cdot 2H_2O$, >98%) was obtained from Sigma-Aldrich and Mallinckrodt. Zinc acetate dihydrate ($Zn(OAc)_2 \cdot 2H_2O$, 98%+) was obtained from Strem Chemicals. *n*-Octylamine (99%), oleylamine (70%), 1-octadecene (90%), oleic acid (90%), toluene (CHROMASOLV for HPLC, 99.9%), methanol (ACS Reagent, ≥99.8%), and dichloromethane (CHROMASOLV for HPLC, 99.8%) were obtained from Sigma-Aldrich. All reagents were used as received. TEM sample grids (Cu with holey carbon film) were obtained from Ted Pella, Inc.

The {CdSe[*n*-octylamine]$_x$} quantum belts (QBs)[20] and {CdS[*n*-octylamine]$_p$} quantum platelets (QPs)[19] were prepared as previously

reported. All synthetic procedures were conducted under an ambient atmosphere unless otherwise indicated.

Analyses. UV−visible spectra were obtained from a PerkinElmer Lambda 950 UV/vis spectrometer or a Varian Cary 100 Bio UV−visible spectrophotometer. Photoluminescence (PL) spectra were collected using a Varian Cary Eclipse fluorescence spectrophotometer. XRD patterns were obtained from a Bruker d8 Advance X-ray diffractometer. Low-resolution TEM images were obtained from a JEOL 2000FX microscope operating at 200 kV. IR spectra were obtained from a PerkinElmer Spectrum BX FT-IR system. Elemental analyses (Table 1; C, H, and N) were obtained from Galbraith Laboratories, Inc. (Knoxville, TN).

Table 1. Elemental Analysis Data Collected from Several Specimens from Different Synthetic Batches[a]

{CdSe[*n*-octylamine]$_{0.53}$}	%C	%H	%N	washing procedure
calcd	19.59	3.90	2.86	
found (1)	21.35	4.02	3.21	toluene (6×)
found (2)	30.77	5.49	2.69	toluene (6×)
found (3)	19.37	3.66	2.79	toluene/methanol (3×), toluene (3×)
found (4)	18.20	3.41	2.60	toluene/methanol (3×), toluene (3×)
{CdSe[Cd(oleate)$_2$]$_{0.19}$}				
calcd	25.70	3.95	0	
found (1)	33.05	5.14	<0.5	toluene/methanol (3×)
found (2)	26.12	3.68	<0.5	toluene (5×)
found (3)	26.04	3.84	<0.5	toluene/methanol (1×), toluene (3×)
found (4)	25.95	3.80	<0.5	toluene/methanol (1×), toluene (3×)

[a]See Results and Supporting Information, Tables S1 and S2. Each analytical specimen of {CdSe[*n*-octylamine]$_{0.53}$} or {CdSe[Cd-(oleate)$_2$]$_{0.19}$} was approximately 18−22 mg, and each washing step was conducted with approximately 3 mL of solvent. The values in parentheses indicate the number of washing steps.

Preparation of an Anhydrous $Cd(oleate)_2$ Solution. In a typical procedure, $Cd(OAc)_2 \cdot 2H_2O$ (69 mg, 0.26 mmol) and oleic acid (147 mg, 0.52 mmol) were dissolved in 1-octadecene (1.5 g) in a septum-capped test tube that was transferred to a 120 °C oil bath for 20 min to achieve a colorless, viscous solution. The tube was then shaken vigorously a few times and heated under vacuum (200 mTorr) at 120 °C for 20 min to remove water and acetic acid. The concentration of the resulting $Cd(oleate)_2$ solution was determined to be 0.11 M by integration against an internal standard using ^1H NMR (NMR spectrum and relevant calculations are provided in Supporting Information, Figure S1).

Preparation of an Anhydrous $Zn(oleate)_2$ Dispersion. In a typical procedure, $Zn(OAc)_2 \cdot 2H_2O$ (57 mg, 0.26 mmol) and oleic acid (147 mg, 0.52 mmol) were dissolved in 1-octadecene (1.5 g) in a septum-capped test tube that was transferred to a 120 °C oil bath for 30 min. The solution became colorless and viscous, with a small amount of white solid remaining on the bottom of the tube. The tube was then heated under vacuum (200 mTorr) at 120 °C for 20 min to remove water and acetic acid. The clear and colorless supernatant was transferred to another test tube, and the remaining solid was discarded. The $Zn(oleate)_2$ solution remained colorless while hot, but a white precipitate formed, giving a cloudy suspension, upon cooling. The mixture was shaken before use to provide a uniform dispersion. An effective concentration of 0.13 M was assumed by the reagent quantities employed.

Preparation of a Stock Mixture of {CdSe[*n*-octylamine]$_x$} QBs. The synthesis of {CdSe[*n*-octylamine]$_x$} QBs was conducted on the same scale as that previously reported[20] (corresponding to 0.27 mmol of $Cd(OAc)_2 \cdot 2H_2O$ and 0.47 mmol of selenourea). The yellow

dispersion obtained after TOP addition was stored under N_2 at room temperature for use as a stock mixture.

Preparation of a Stock Mixture of {CdS[*n*-octylamine]$_p$} QPs. The synthesis of {CdS[*n*-octylamine]$_p$} QPs was conducted on the same scale as that previously reported[19] (corresponding to 0.20 mmol of Cd(OAc)$_2$·2H$_2$O and 0.40 mmol of thioacetamide). After the reaction mixture was stored at 0 °C overnight, the bundled {CdS[*n*-octylamine]$_p$} QPs precipitated as a yellowish white solid under a colorless supernatant. The QPs were redispersible by vigorous shaking. This dispersion was stored under N_2 at room temperature for use as a stock mixture.

Surface Exchange of {CdSe[*n*-octylamine]$_x$} QBs with Cd-(oleate)$_2$. An aliquot (0.2 mL) of the CdSe QB stock mixture was transferred to a septum-capped test tube, and toluene (1 mL) was added. The resulting pale-yellow precipitate was separated by a benchtop centrifuge (1500 rpm, 5 min), and the supernatant was discarded. The dispersion−centrifugation cycle was repeated two additional times. The purpose of this purification process was to remove excess *n*-octylamine.

Anhydrous Cd(oleate)$_2$ solution (1 mL) was added to the purified {CdSe[*n*-octylamine]$_x$} QBs, resulting in a clear, bright-yellow solution of {CdSe[Cd(oleate)$_2$]$_y$} instantaneously upon mixing. Two drops of {CdSe[Cd(oleate)$_2$]$_y$} were taken to obtain a PL spectrum.

Subsequent analyses were conducted using purified {CdSe[Cd-(oleate)$_2$]$_y$}. Toluene (1.5 mL) and methanol (0.5 mL) were added to the CdSe[Cd(oleate)$_2$]$_y$} solution, resulting in a bright-yellow precipitate, which was collected after centrifugation (4500 rpm, 5 min). This precipitate was used for UV−vis and XRD analyses. For FT-IR analysis, the toluene−methanol dispersion and centrifugation cycle was conducted two additional times to ensure removal of free ligands.

Surface Exchange of {CdS[*n*-octylamine]$_p$} QPs with Cd-(oleate)$_2$. The same procedure as that described above for the CdSe QBs was employed. The yellowish-white CdS QP dispersion became more transparent upon addition of the anhydrous Cd(oleate)$_2$ solution. The exchanged {CdS[Cd(oleate)$_2$]$_q$} QPs were collected as a white precipitate after the purification step.

Surface Exchange of {CdSe[*n*-octylamine]$_x$} QBs and {CdS[*n*-octylamine]$_p$} QPs with Zn(oleate)$_2$. Aliquots from the CdSe QB and CdS QP stock mixtures were purified as above. The purified CdSe QB or CdS QP solids were dispersed in toluene (1 mL) to form cloudy suspensions. Separately, the Zn(oleate)$_2$ stock suspension was well-mixed by stirring to form a viscous white mixture. The Zn(oleate)$_2$ suspension was added to the CdSe QB or CdS QP dispersions drop by drop in a total amount of 16 drops. The cloudy pale-yellow CdSe dispersion gradually turned clearer and brighter upon addition of Zn(oleate)$_2$, and it became completely clear in 0.5−1 min. The cloudy CdS dispersion became almost clear in 1 min upon addition of Zn(oleate)$_2$.

The resulting {CdSe[Zn(oleate)$_2$]$_m$} dispersion was purified once as described above for {CdSe[Cd(oleate)$_2$]$_y$}. The {CdS[Zn(oleate)$_2$]$_n$} dispersion was purified in the same manner.

Back Exchange of {II−VI[M(oleate)$_2$]$_f$} QBs/QPs to {II−VI[amine]$_g$} QBs/QPs. Back exchange was conducted using both the initial {CdSe[Cd(oleate)$_2$]$_y$} solution or the purified {CdSe[Cd-(oleate)$_2$]$_y$} solid. Addition of *n*-octylamine (or oleylamine, 1.5 mL) converted the bright-yellow solid or solution to a pale-yellow color. Two drops of the resulting {CdSe[*n*-octylamine]$_{x'}$} or ({CdSe-[oleylamine]$_{z'}$}) solution were taken to obtain PL spectra. Subsequent analyses were conducted after purification as described above for the M(oleate)$_2$-passivated QBs/QPs (M = Cd, Zn). Back exchange of the other {II−VI[M(oleate)$_2$]$_f$} QBs/QPs was conducted similarly.

■ RESULTS

Reversible Spectroscopic Changes Accompanying Exchange of L- and Z-Type Passivation in CdSe QBs. The synthesis of amine-passivated CdSe QBs was previously reported.[20] A UV−visible extinction spectrum of as-synthesized CdSe QBs passivated by *n*-octylamine, {CdSe[*n*-octylamine]$_x$},

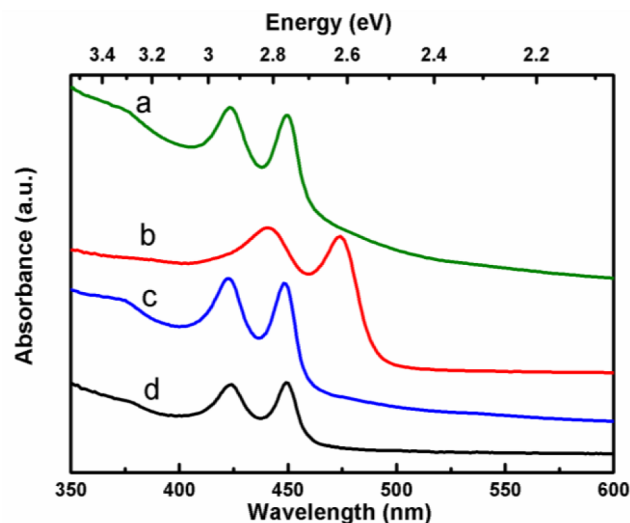is given in Figure 1a. These QBs were previously shown to possess the wurtzite structure, with the thickness dimension

Figure 1. UV−visible extinction spectra (in toluene dispersion at RT) of (a) starting {CdSe[*n*-octylamine]$_x$}, (b) {CdSe[Cd(oleate)$_2$]$_y$}, (c) back-exchanged {CdSe[*n*-octylamine]$_{x'}$}, and (d) back-exchanged {CdSe[oleylamine]$_{z'}$}.

oriented along [1 1 −2 0], the width along [1 −1 0 0], and the length along [0 0 0 1]. The QBs had discrete thicknesses of 1.8 nm (corresponding to five monolayers of CdSe),[18] establishing the confinement dimension, and sample-dependent widths and lengths in the ranges of 10 ± 5 nm and 1 ± 0.5 μm, respectively.[20] The spectrum of the QBs (Figure 1a) contained three absorption features, previously assigned to quantum-well transitions.[18] The lowest-energy feature appeared at 449 nm (2.76 ± 0.01 eV).

Washed {CdSe[*n*-octylamine]$_x$} QBs were combined with anhydrous Cd(oleate)$_2$ in ODE solvent. The color of the dispersion changed from pale-yellow to bright-yellow instantaneously upon mixing at room temperature. An extinction spectrum of the resulting {CdSe[Cd(oleate)$_2$]$_y$} QBs is given in Figure 1b. The QB absorption features were shifted to lower energy. The lowest-energy feature was shifted by 24 nm (140 ± 20 meV) to 473 nm (2.62 ± 0.01 ev), and the second feature was also shifted by a significant amount. The third, weakest feature was broadened and obscured after the change in surface passivation.

Addition of primary amine to {CdSe[Cd(oleate)$_2$]$_y$} QB dispersions was found to reverse these spectroscopic shifts. A {CdSe[Cd(oleate)$_2$]$_y$} dispersion and *n*-octylamine reacted instantaneously to restore a cloudy, pale-yellow {CdSe[*n*-octylamine]$_{x'}$} dispersion giving the extinction spectrum in Figure 1c. The lowest-energy QB feature appeared at 449 nm, and the third, weakest feature reappeared at its original position. Similarly, a {CdSe[Cd(oleate)$_2$]$_y$} dispersion and oleylamine reacted instantaneously to generate a clear, pale-yellow solution (dispersion) giving the extinction spectrum in Figure 1d. The QB absorption features were restored to similar, higher-energy positions (449, 423, and 375 nm). The lowest-energy λ_{max} values, spectral shifts, and energy shifts associated with the variously passivated CdSe QBs are summarized in Table 2.

The reversible shifting observed in the extinction spectra was paralleled by corresponding changes in the photoluminescence

Table 2. Lowest-Energy λ_{max} Values, Spectral Shifts, and Energy Shifts Associated with the Variously Passivated CdSe QBs

QB/QP	λ_{max} (nm)[a]	$\Delta\lambda_{max}$ (nm)[b]	ΔE (meV)
{CdSe[n-octylamine]$_{0.53}$}	449 ± 1	0	0
{CdSe[Cd(oleate)$_2$]$_{0.19}$}	473 ± 1	24 ± 2	140 ± 20
{CdSe[Zn(oleate)$_2$]$_m$}	454 ± 1	5 ± 2	30 ± 20
{CdS[n-octylamine]$_p$}	373 ± 1	0	0
{CdS[Cd(oleate)$_2$]$_q$}	384 ± 1	11 ± 2	90 ± 20
{CdS[Zn(oleate)$_2$]$_n$}	379 ± 1	6 ± 2	50 ± 20

[a]For the lowest-energy absorption feature. [b]Relative to the n-octylamine-passivated QB or QP.

(PL) spectra. As discussed previously,[18] amine-passivated 2D II−VI nanocrystals exhibit strong, sharp emission features, which are minimally Stokes-shifted from the lowest-energy absorptions. Thus, the as-synthesized {CdSe[n-octylamine]$_x$} QBs gave the PL spectrum in Figure 2a, having a λ_{max} at 452
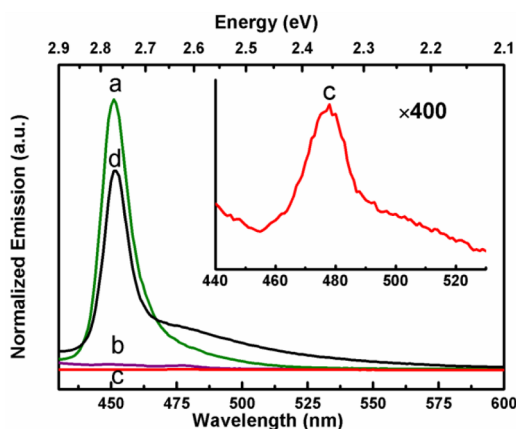

Figure 2. PL spectra (in toluene dispersion, at RT) of (a) as-synthesized {CdSe[n-octylamine]$_x$} (green), (b) {CdSe[n-octylamine]$_x$} after removal of excess n-octylamine (purple), (c) as-synthesized {CdSe[Cd(oleate)$_2$]$_y$} (red), and (d) back-exchanged {CdSe[oleylamine]$_{z'}$} (black). The inset is a vertical expansion of (c).

nm. The PL intensity was largely quenched by the washing step to remove excess n-octylamine, which preceded surface exchange (Figure 2b). The PL spectrum remained very weak in the exchanged {CdSe[Cd(oleate)$_2$]$_y$} product, but it gave a discernible feature at λ_{max} = 479 nm (Figure 2c). Replacement of the Cd(oleate)$_2$ surface passivation by oleylamine passivation restored the PL intensity and shifted λ_{max} back to 452 nm (Figure 2d). The emission feature in the back-exchanged oleylamine-passivated QBs exhibited a prominent low-energy shoulder, presumably indicative of surface traps introduced during the ligand-exchange process.

If exchanges in CdSe QB surface passivation were indeed responsible for the reversible spectral shifting described above, then the overall morphologies of the QBs should not be greatly affected by the exchange process. Figure 3a is a TEM image of the starting {CdSe[n-octylamine]$_x$} QBs after unbundling with oleylamine (see ref 20). The mean width and length of the QBs were 6 ± 1 nm and 335 ± 70 nm, respectively. Figure 3b is a corresponding image of the {CdSe[Cd(oleate)$_2$]$_y$} QBs resulting from surface exchange with Cd(oleate)$_2$, in which the mean width was 7 ± 1 nm and the mean length had decreased to 271 ± 79 nm. Figure 3c is an image of the
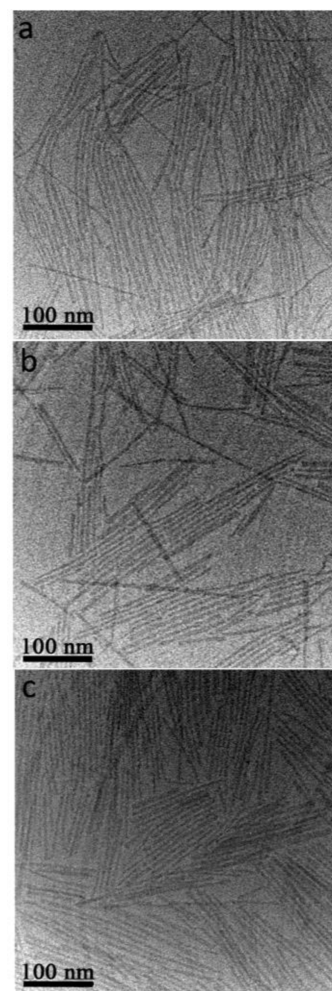

Figure 3. TEM images of (a) starting {CdSe[n-octylamine]$_x$} after unbundling with oleylamine, (b) {CdSe[Cd(oleate)$_2$]$_y$}, and (c) back-exchanged {CdSe[oleylamine]$_{z'}$}.

{CdSe[oleylamine]$_{z'}$} QBs back-exchanged to amine passivation, in which the mean width was 6 ± 1 nm and the mean length had further decreased to 236 ± 52 nm (HRTEM images of CdSe QBs before and after ligand exchange are provided in Supporting Information, Figure S3).

Apart from the progressive decrease in mean length, the QBs underwent no distinct morphological changes as a result of the exchange process. The decrease in length may have been due to cleavage resulting from changes in the strain states of the QBs (see below) or merely to mechanical intercontact during the physical manipulations. Note that the changes in length did not influence the spectroscopic properties of the QBs, as length is not a confinement dimension. The results were consistent with a QB surface-exchange process.

Characterization of L- and Z-Passivated CdSe QBs. The identities of the surface-bound ligands were examined by IR spectroscopy. The IR spectrum of the starting {CdSe[n-octylamine]$_x$} QBs contained three distinct N−H stretches in the range of 3330−3132 cm^{-1} diagnostic of primary-amine passivation (Figure 4a). Upon surface exchange to {CdSe[Cd(oleate)$_2$]$_y$}, the N−H stretches disappeared and asymmetric and symmetric CO$_2$ stretches appeared at 1536 and 1412 cm^{-1}, respectively (Figure 4b). The resulting Δ value, 1536 cm^{-1} − 1412 cm^{-1} = 124 cm^{-1}, in comparison to Δ = 128 cm^{-1} for

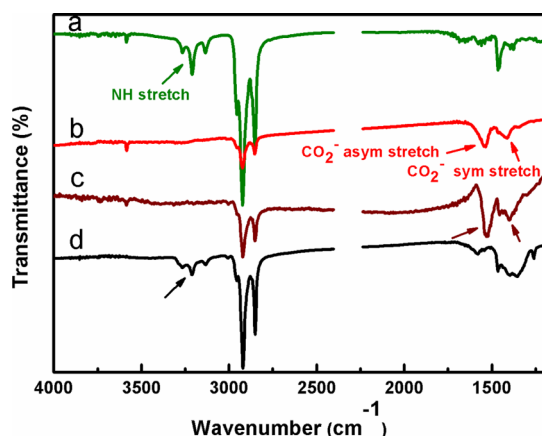**Figure 4.** IR spectra (from KBr pellets) of (a) starting $\{CdSe[n\text{-}octylamine]_x\}$, (b) $\{CdSe[Cd(oleate)_2]_y\}$, (c) $\{CdSe[Zn(oleate)_2]_m\}$, and (d) back-exchanged $\{CdSe[oleylamine]_{z'}\}$ from (b). N–H stretches are identified by arrows in (a) and (d); asymmetric and symmetric CO_2 stretches are identified in (b) and (c).

sodium oleate, was indicative of bridging carboxylate ligands.[21] Asymmetric and symmetric CO_2 stretches were also observed at 1528 and 1400 cm^{-1} ($\Delta = 128$ cm^{-1}) in the IR spectrum of zinc-carboxylate-passivated $\{CdSe[Zn(oleate)_2]_m\}$ QBs (discussed below; Figure 4c). The latter Δ value was also indicative of bridging oleate ligands. Back exchange to oleylamine-passivated $\{CdSe[oleylamine]_{z'}\}$ QBs restored the N–H stretches to the IR spectrum and removed the CO_2 features (Figure 4d). Thus, the IR analysis supported the surface-exchange processes claimed above.

Low-angle XRD provided a second means of characterizing the QB surface exchange. The QBs exhibit a strong tendency to bundle into pseudoparallel alignment, having their broad top and bottom surfaces stacked together, so precipitated QB solids give low-angle 00l reflections corresponding to the lamellar spacings in these bundles. These interlayer spacings correspond to the sum of thicknesses of the QBs and the ligand bilayers separating them. XRD patterns obtained from the initial $\{CdSe[n\text{-}octylamine]_x\}$ QBs, the exchanged $\{CdSe[Cd(oleate)_2]_y\}$ QBs, and the back-exchanged $\{CdSe[n\text{-}octylamine]_{x'}\}$ and $\{CdSe[oleylamine]_{z'}\}$ QBs are recorded in Figure 5. The interlayer (d) spacings calculated from these patterns are given in Table 3.

We considered that differences in the d spacings of the variously passivated QBs should be largely determined by the lengths of the alkyl chains on the surface-bound species. Thus, the d spacings for the n-octylamine-passivated QBs (Table 3) were 2.51 and 2.68 nm, respectively, before and after a surface-exchange cycle. The small difference in these values likely reflects various degrees of disordering in the bundled QB assemblies. Both of these d spacings were consistent with other, related n-octylamine-bilayer mesophases ($d = 2.5$–2.8 nm).[20,22] Exchange to oleylamine or $Cd(oleate)_2$ passivation expanded the observed d spacings to 4.65 and 4.66 nm, respectively, reflecting the increased length of the 18-carbon chains vs the 8-carbon alkyl chain of n-octylamine. Thus, the QB spacings within their aggregated bundles determined by low-angle XRD were consistent with the proposed surface-exchange processes.

The variously passivated CdSe QBs were also characterized by elemental analysis. Four samples of $\{CdSe[n\text{-}octylamine]_x\}$ were analyzed, producing the results recorded in Table 1. These samples were obtained from different synthetic batches and
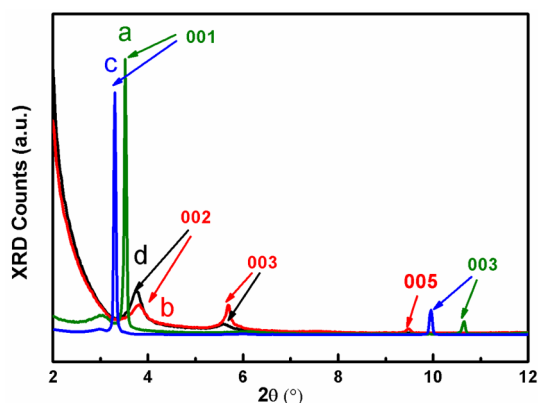

Figure 5. Low-angle XRD patterns of (a) starting $\{CdSe[n\text{-}octylamine]_x\}$ (green), (b) $\{CdSe[Cd(oleate)_2]_y\}$ (red), (c) back-exchanged $\{CdSe[n\text{-}octylamine]_{x'}\}$ (blue), and (d) back-exchanged $\{CdSe[oleylamine]_{z'}\}$ (black). The lamellar 00l reflections are indexed.

Table 3. Interlamellar d Spacings in Variously Passivated CdSe QBs

variously passivated CdSe QBs	d spacing (nm)
$\{CdSe[n\text{-}octylamine]_x\}$	2.51
$\{CdSe[Cd(oleate)_2]_y\}$	4.66
$\{CdSe[n\text{-}octylamine]_{x'}\}$	2.68
$\{CdSe[oleylamine]_{z'}\}$	4.65

were washed by slightly different methods to remove excess n-octylamine. One of the analyses differed markedly from the other three (Table 1). The rejection quotient for this analysis $Q = 0.75$ was close to $Q_{90} = 0.76$; thus, it was rejected with a confidence near 90% (see Table S1 and associated calculations). The formula $\{CdSe[n\text{-}octylamine]_{0.53}\}$ (or $x = 0.53 \pm 0.06$) was obtained by averaging the results of the three consistent analyses.

Similarly, four samples of $\{CdSe[Cd(oleate)_2]_y\}$ were analyzed, giving the results in Table 1. These samples were obtained by surface exchange of the four batches of $\{CdSe[n\text{-}octylamine]_{0.53}\}$ used for the analyses above and were washed by slightly different methods. Again, one analysis was an outlier. This analysis gave a $Q = 1$, in excess of $Q_{99} = 0.93$, and thus was rejected with a confidence of 99% (see Table S2 and associated calculations). The average composition of $\{CdSe[Cd(oleate)_2]_{0.19}\}$ ($y = 0.19 \pm 0.02$) was determined from the remaining three analyses. Significantly, nitrogen was below the detection limit in all four specimens, establishing the complete removal of n-octylamine by the exchange process. Therefore, CdSe QB characterization by IR spectroscopy, low-angle XRD, and elemental analyses confirmed the surface-exchange processes proposed above. The empirical formulas determined by elemental analysis are used later to determine surface coverages.

Additional Examples of Reversible Exchange of L- and Z-Type Passivation. A related surface exchange between $\{CdSe[n\text{-}octylamine]_{0.53}\}$ QBs and anhydrous $Zn(oleate)_2$ was undertaken, which required about 30 s at room temperature, and afforded $\{CdSe[Zn(oleate)_2]_m\}$ QBs. The UV–visible extinction spectrum of this exchange product in Figure 6b is compared to those of $\{CdSe[n\text{-}octylamine]_{0.53}\}$ and $\{CdSe[Cd(oleate)_2]_{0.19}\}$ QBs (Figure 6, panels a and c, respectively). The absorption features of the $\{CdSe[Zn(oleate)_2]_m\}$ QBs were shifted to lower energy than those of the amine-passivated
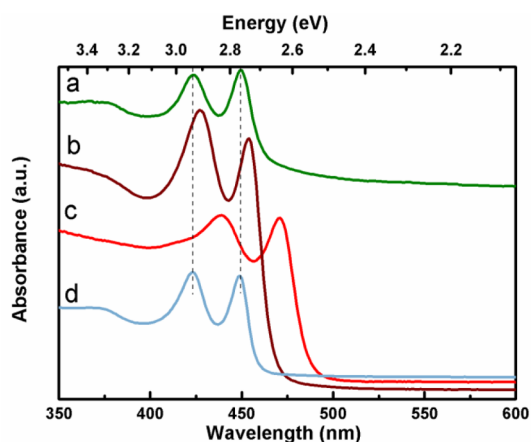
Figure 6. UV−visible extinction spectra (in toluene dispersion at RT) of (a) starting {CdSe[n-octylamine]$_{0.53}$}, (b) {CdSe[Zn(oleate)$_2$]$_m$}, (c) {CdSe[Cd(oleate)$_2$]$_{0.19}$}, and (d) back-exchanged {CdSe[n-octylamine]$_{x'}$} from (b).

{CdSe[n-octylamine]$_{0.53}$}, with the lowest-energy feature shifted by 5 nm (30 ± 20 meV). Thus, the shifts were smaller in magnitude than those reported above for {CdSe[Cd-(oleate)$_2$]$_{0.19}$}, but they were in the same direction. Back exchange of the CdSe[Zn(oleate)$_2$]$_m$} QBs to {CdSe[n-octylamine]$_{x'}$} by exposure to excess n-octylamine gave the spectrum in Figure 6d, which matched that of the starting {CdSe[n-octylamine]$_{0.53}$} QBs, establishing that the surface-exchange process was again reversible.

Additional experiments were conducted with amine-passivated CdS quantum platelets (QPs), {CdS[n-octylamine]$_p$}, prepared by a method we previously reported.[19] (TEM images are provided in the Supporting Information, Figure S4.) These QPs had discrete thicknesses of 1.5 nm, widths of ≈5 nm, and lengths in the range of 30−40 nm.[19] The UV−visible extinction spectrum of the QPs (Figure 7a) contained two features: a strong absorption at 373 nm and a weaker absorption at 337 nm. Two features were observed, rather than the three features exhibited by the CdSe QBs (Figure 1), because the light- and heavy-hole transitions are not resolved in CdS QPs of such small thickness.[19] The spectrum also
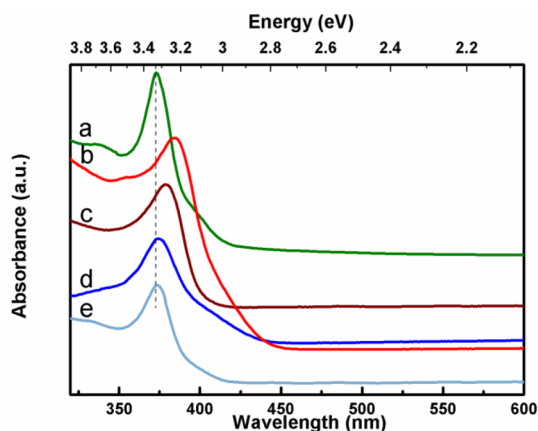

Figure 7. UV−visible extinction spectra (in toluene dispersion at RT) of (a) starting {CdS[n-octylamine]$_p$}, (b) {CdS[Cd(oleate)$_2$]$_q$}, (c) {CdS[Zn(oleate)$_2$]$_n$}, (d) back-exchanged {CdS[n-octylamine]$_{p'}$} from (b), and (e) back-exchanged {CdS[n-octylamine]$_{p'}$} from (c).

contained a weak shoulder near 400 nm, which has not been assigned.

Addition of anhydrous Cd(oleate)$_2$ to the {CdS[n-octylamine]$_p$} QPs at room temperature resulted in an instantaneous shift of the prominent lower-energy absorption from 373 to 384 nm, a shift of 90 ± 20 meV (Figure 7b), upon surface exchange to {CdS[Cd(oleate)$_2$]$_q$}. Similarly, surface exchange between {CdS[n-octylamine]$_p$} and Zn(oleate)$_2$ resulted in shift of this feature to 379 nm (by 50 ± 20 meV; Figure 7c) upon formation of {CdS[Zn(oleate)$_2$]$_n$}. The spectra for both of the carboxylate-passivated QP derivatives were returned to that of the initial {CdS[n-octylamine]$_{p'}$} QPs upon back exchange by addition of n-octylamine (Figure 7d,e). The results established that CdS QPs were also capable of reversible surface exchange. The lowest-energy λ_{max} values, spectral shifts, and energy shifts associated with the variously passivated CdS QPs are summarized in Table 2.

The IR spectra of the CdS QPs are given in Figure 8. The spectrum of {CdS[n-octylamine]$_p$} (Figure 8a) contains N−H
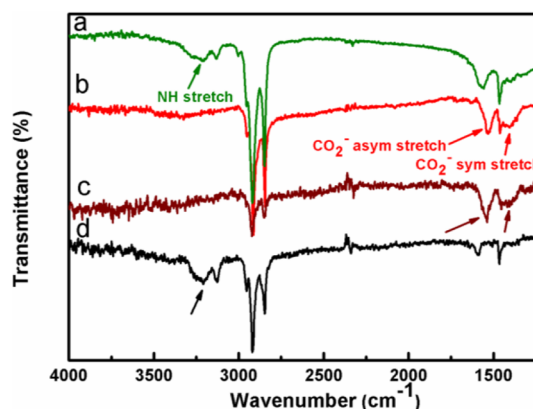

Figure 8. IR spectrum of (a) starting {CdS[n-octylamine]$_p$}, (b) {CdS[Cd(oleate)$_2$]$_q$}, (c) {CdS[Zn(oleate)$_2$]$_n$}, and (d) back-exchanged {CdS[oleylamine]$_{r'}$} from (b). N−H stretches are identified by arrows in (a) and (d); asymmetric and symmetric CO$_2$ stretches are identified in (b) and (c).

stretching vibrations in the expected range (3300−3130 cm^{-1}). These N−H stretches are absent in the IR spectra of {CdS[Cd(oleate)$_2$]$_q$} and {CdS[Zn(oleate)$_2$]$_n$} (Figure 8b,c) and are replaced by asymmetric CO$_2$ stretches at 1532 and 1538 cm^{-1} and symmetric CO$_2$ stretches at 1406 and 1404 cm^{-1}, respectively, close to the positions of the corresponding vibrations in {CdSe[Cd(oleate)$_2$]$_{0.19}$} and {CdSe[Zn-(oleate)$_2$]$_m$} QBs reported above (Figure 4). The resulting Δ values again established bridging coordination modes for the oleate ligands in both cases.[21] Back exchange of {CdS[Cd-(oleate)$_2$]$_q$} to the L-type {CdS[oleylamine]$_r$} restored the N−H stretches and removed the CO$_2$ stretches (Figure 8d). Thus, the IR data confirmed the surface exchanges in these additional examples.

Analysis of Lattice Strain in the 2D II−VI Nanocrystals. As noted in the Introduction, lattice strain influences the effective band gaps of semiconductor nanocrystals. This lattice strain results from surface reconstruction and passivation and may be either compressive or tensile in character, producing lattice contractions or dilations, respectively.[17,18,23,24] We[25,26] and others[27−29] previously reported lattice contractions of up to 6.5% in amine-passivated 2D II−VI nanocrystals having wurtzite structures. Contractions were observed in both a and

c lattice parameters, but they were larger in the thickness dimension of the 2D nanocrystals. Because *a* has a component in the thickness dimension, whereas *c* does not (lying parallel to the long dimension of the QB or QP),[18] the percent contractions, determined from XRD data, were greater in *a*. Consequently, we considered that changes in the strain states of the QBs and QPs accompanying the changes in surface passivation from L- to Z-type may have been responsible for the reversible spectral shifting detailed above.

High-angle XRD data obtained from the variously passivated CdSe QBs, in the range of the first three (100, 002, and 101) reflections, are plotted in Figure 9. These reflections were
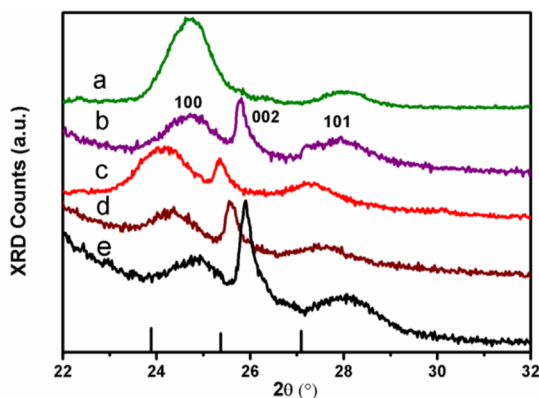

Figure 9. High-angle XRD data from (a) starting {CdSe[*n*-octylamine]$_{0.53}$}, (b) {CdSe[oleylamine]$_z$}, (c) {CdSe[Cd-(oleate)$_2$]$_{0.19}$}, (d) {CdSe[Zn(oleate)$_2$]$_m$}, and (e) back-exchanged {CdSe[oleylamine]$_{z'}$} from (c) in the range of the first three (100, 002, and 101) reflections. The black lines on the *x* axis are the positions of these reflections in bulk CdSe.

shifted relative to one another and from the bulk values by lattice contractions. For example, the 100 reflection in unstrained, bulk CdSe appears at 23.8° 2*θ*, whereas that in the {CdSe[oleylamine]$_z$} QBs appeared at 24.7° 2*θ* (Figure 9b).

We note that the 002 reflection is missing from the XRD pattern of the {CdSe[*n*-octylamine]$_{0.53}$} QBs (Figure 8a). This absence is due to the tightly bundled nature of the *n*-octylamine derivative, which preferentially oriented the long axis of the QBs in the substrate plane, removing the (002) planes from the diffraction condition. However, the 100 and 101 reflections of the {CdSe[*n*-octylamine]$_{0.53}$} and {CdSe[oleylamine]$_z$} QBs appeared at nearly the same angle 2*θ*, indicating that the primary-amine (L-type) passivation induced similar lattice contractions in both specimens.

The values of the lattice contractions were determined from the positions of the 100 and 002 reflections for the variously passivated CdSe QBs (Table 4). The results indicated higher strain (larger contractions) in the L-type amine-passivated QBs than in the Z-type metal-carboxylate-passivated QBs.

Two patterns are provided for {CdSe[oleylamine]$_{z,z'}$} QBs. The specimen used for Figure 9b was obtained by surface exchange from {CdSe[*n*-octylamine]$_{0.53}$}, and the specimen used for Figure 9e was obtained by back exchange from {CdSe[Cd(oleate)$_2$]$_{0.19}$}. The lattice contractions determined for the two specimens were similar but not identical (Table 4). Their similarity established that changes in the strain states resulting from surface exchange were largely reversible.

Table 4. Values of the Lattice Parameters and Strain States of Variously Passivated 2D II−VI Nanocrystals

QB/QP specimens	*a* (Å)	contraction in *a* (%)	*c* (Å)	contraction in *c* (%)
{CdSe[*n*-octylamine]$_{0.53}$}	4.15	3.4 ± 0.1	6.90	1.6
{CdSe[oleylamine]$_z$}	4.15	3.4 ± 0.1	6.90	1.6
{CdSe[Cd(oleate)$_2$]$_{0.19}$}	4.26	0.9 ± 0.3	7.02	0
{CdSe[Zn(oleate)$_2$]$_m$}	4.22	1.9 ± 0.1	6.97	0.7
{CdSe[oleylamine]$_{z'}$}	4.13	4.0 ± 0.1	6.88	2.0
{CdS[*n*-octylamine]$_p$}	3.99	3.3 ± 0.2	6.61	2.1
{CdS[Cd(oleate)$_2$]$_q$}	4.08	1.2 ± 0.2	6.70	0.7
{CdS[Zn(oleate)$_2$]$_n$}	4.08	1.2 ± 0.1	6.68	1.0

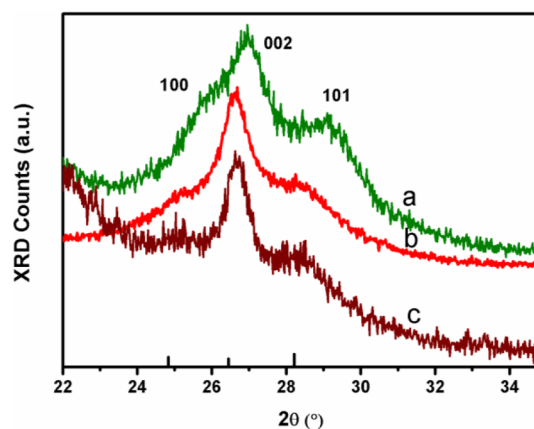High-angle XRD data for the variously passivated CdS QPs are given in Figure 10, and the corresponding lattice

Figure 10. High-angle XRD data from (a) starting {CdS[*n*-octylamine]$_p$}, (b) {CdS[Cd(oleate)$_2$]$_q$}, and (c) {CdS[Zn-(oleate)$_2$]$_n$} in the range of the first three (100, 002, and 101) reflections.

contractions are recorded in Table 4. Because the 100 reflections are not well-resolved in these patterns, the lattice parameters were calculated using the positions of the 002 and 101 reflections. The magnitudes of the lattice contractions in the CdS QPs were quite similar to the correspondingly passivated CdSe QBs. As for the CdSe QBs, the lattice contractions were larger and the compressive strains were higher in the L-type amine-passivated CdS QPs than in the Z-type metal-carboxylate-passivated CdS QPs. The contribution of changes in the strain states to the reversible spectral shifts is analyzed in the Discussion.

Surface Coverage in CdSe QBs. The elemental analysis data and mean QB dimensions allowed calculations of the average surface coverages of the CdSe QBs to be performed. Figure 11 represents a view perpendicular to the small end facet of a QB. From this perspective, the structure is bounded by the broad top and bottom facets at the top and bottom of the lattice and by the thin, long edge facets on the left and right edges.[18] The thickness dimension is oriented vertically. We defined one crystallographic monolayer in the quantum-confined thickness dimension as the thinnest layer constituting a contiguously bonded net,[18] and the top and bottom monolayers are so identified in Figure 11. The monolayers are nominally corrugated (if unreconstructed), consisting of parallel, alternating ridges and valleys (like corduroy) on the top and bottom facets, running perpendicular to the plane of the figure.
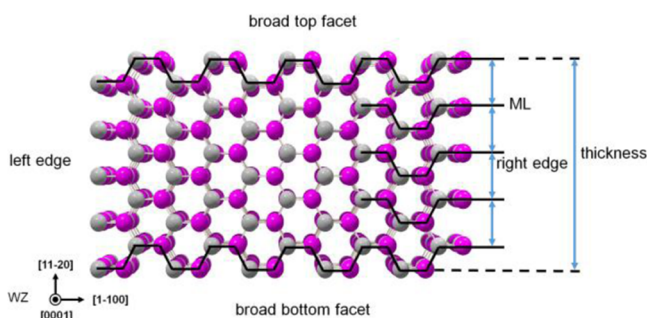
Figure 11. View perpendicular to the small end facet of a QB. Cd and Se atoms are gray and magenta, respectively.

The CdSe QBs used in this study had a discrete thickness of 1.8 nm, or five CdSe monolayers. Thus, the two monolayers forming the top and bottom facets account for 40% of the CdSe in the QBs, or 40% of the Cd and Se atoms in the QBs are on the broad top and bottom surfaces. Notably, the Cd and Se atoms in the surface valley positions are nominally four-coordinate, whereas those in the surface ridge positions are nominally three-coordinate, prior to surface-ligand coordination.

The overall composition of the amine-passivated QBs was determined to be $\{CdSe[n\text{-octylamine}]_{0.53\pm0.06}\}$ (see above). If an n-octylamine ligand was bonded to each Cd atom on the top and bottom QB facets, in both the ridge and valley positions, then the composition would be $\{CdSe[n\text{-octylamine}]_{0.40}\}$. Alternatively, if an n-octylamine ligand was bonded to each Cd and each Se atom in the ridge positions of the top and bottom facets, then the composition would be $\{CdSe[n\text{-octylamine}]_{0.40}\}$ (that is, the same as above). These alternatives are analyzed in the Discussion.

The thin edge facets of the CdSe QBs are also nonpolar surfaces with structures related to the top and bottom facets. We considered that n-octylamine may be bound to those facets as well. Because the ratio of the mean thickness to mean width of the QBs was 1.8:6.0, an additional 12% of the Cd and Se

atoms were on the edge facets. By the arguments above, n-octylamine coordination to these surfaces, in addition to the top and bottom surfaces, would result in the composition $\{CdSe[n\text{-octylamine}]_{0.40+0.12}\}$ or $\{CdSe[n\text{-octylamine}]_{0.52}\}$, well within the error of the elemental analysis results. This analysis ignored the small relative areas of the two end facets of the QBs.

The overall composition of the $Cd(oleate)_2$-passivated QBs was determined to be $\{CdSe[Cd(oleate)_2]_{0.19\pm0.02}\}$ (see above). According to the analysis above, if one $Cd(oleate)_2$ was bonded for every Se atom in a ridge position of the top and bottom QB facets, then the composition would be $\{CdSe[Cd(oleate)_2]_{0.20}\}$. Alternatively, if one $Cd(oleate)_2$ was bonded for every Se atom in a ridge position on the top, bottom, and two edge QB facets, then the composition would be $\{CdSe[Cd(oleate)_2]_{0.26}\}$. These two surface-bonding models provide compositions close to and not likely distinguishable by the elemental analysis results. Again, the small relative areas of the two end facets of the QBs were ignored.

The analyses presented in this section demonstrated that plausible surface-coverage models rationalized the overall compositions determined experimentally.

◼ DISCUSSION

Proposed Surface Structures for Passivated CdSe QBs. The coverage models elucidated above indicate a stoichiometry of one bound n-octylamine ligand for each surface Cd atom in the $\{CdSe[n\text{-octylamine}]_{0.53}\}$ QBs on the top, bottom, and the two edge facets. However, the unreconstructed top and bottom facets contain two types of Cd atoms: those in three-coordinate ridge positions and those in four-coordinate valley positions. Figure 12a provides a view of a top facet in which the valley positions are shaded to distinguish them from the ridge positions. Both the valleys and ridges consist of parallel, zigzag chains of alternating Cd and Se atoms. Coordination of n-octylamine ligands to the three-coordinate ridge Cd atoms is readily imagined, whereas coordination to the valley Cd atoms seems to be less likely
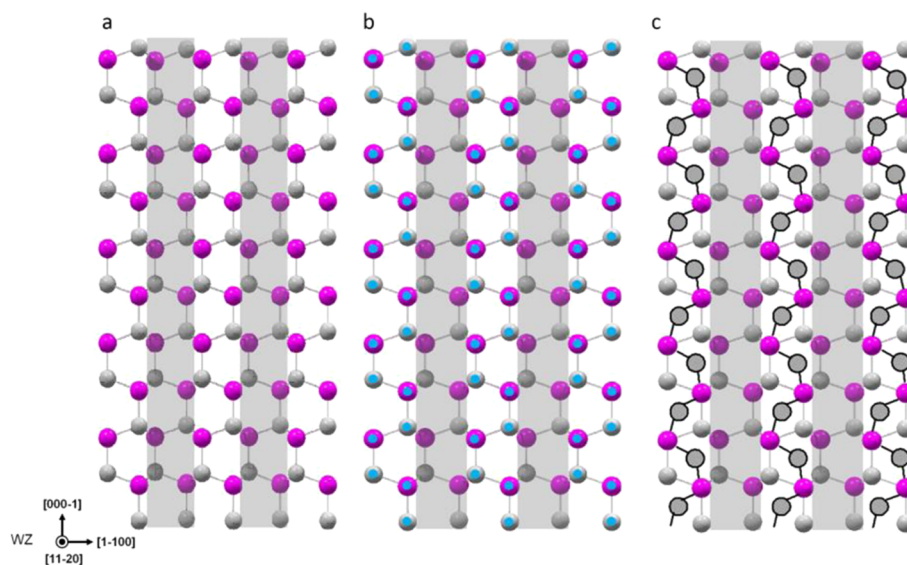

Figure 12. (a) View of a top CdSe QB facet, with the valley positions shaded. (b) Blue dots represent n-octylamine ligands bonded to both Cd and Se atoms in only the ridge positions on a top QB facet. (c) Gray circles (with black borders) represent the proposed coordination of the Cd atoms in the $Cd(oleate)_2$ units to ridge Se atoms in a bridging μ_2 mode on a top QB facet.

Table 5. Observed Spectroscopic Energy Shifts Separated into Strain (ΔE_{strain}) and Confinement Dimension ($\Delta E_{\text{thickness}}$) Components

QB/QP specimen	contraction in a (%)[a]	spectroscopic energy shift (meV)[b]	ΔE_{strain} (meV)[c]	$\Delta E_{\text{thickness}}$ (meV)[d]
{CdSe[n-octylamine]$_{0.53}$}	3.4 ± 0.1	0	0	0
{CdSe[oleylamine]$_z$}	3.4 ± 0.1	0	0	0
{CdSe[Cd(oleate)$_2$]$_{0.19}$}	0.9 ± 0.3	140 ± 20	53 ± 8	87 ± 28
{CdSe[Zn(oleate)$_2$]$_n$}	1.9 ± 0.1	30 ± 20	32 ± 4	0
{CdS[n-octylamine]$_p$}	3.3 ± 0.2	0	0	0
{CdS[Cd(oleate)$_2$]$_q$}	1.2 ± 0.2	90 ± 20	51 ± 7	39 ± 27
{CdS[Zn(oleate)$_2$]$_n$}	1.2 ± 0.1	50 ± 20	51 ± 5	0

[a]From Table 4. [b]From Table 2, relative to the lowest-energy feature in the n-octylamine-passivated QB or QP. [c]Calculated from eq 1. [d]The difference in the spectroscopic energy shift and ΔE_{strain}.

because those atoms are ostensibly tetrahedrally coordinated by lattice atoms, are thus coordinatively saturated, and are much less sterically accessible. Therefore, a structural model for amine passivation in which one n-octylamine ligand is bound to every surface Cd atom is questionable.

A different surface structure is suggested by a recent study of Zhang and co-workers.[30] They analyzed the surface bonding of primary amines to CdSe, ZnSe, and ZnS quantum dots by IR spectroscopy, finding evidence of strong interamine hydrogen bonding among the surface-coordinated ligands. Moreover, the results established the existence of two types of surface-bound primary amines, one of which was selectively removed by methanol substitution. Zhang and co-workers proposed that the two types were amines coordinated to surface Cd atoms and amines coordinated to surface Se atoms, the latter in a hydrogen-bonding-like interaction. In support of that argument, they demonstrated that amine ligands bound only to surface Cd atoms were too widely separated to engage in interamine hydrogen bonding, whereas amines bound to both surface Cd and Se atoms were optimally positioned for hydrogen bonding with one another.

By analogy, we consider n-octylamine bonding to both Cd and Se atoms in only the ridge positions on the top and bottom QB surfaces (Figure 12b), which allows contiguous strips of interamine hydrogen bonding. The edge facets do not have precisely the same ridge-and-valley structure. They lack the Cd–Se zigzag chains but are nonpolar surfaces having an equal number of Cd–Se dimers in ridge three-coordinate environments and valley four-coordinate environments. Consequently, n-octylamine ligands could be bound to both Cd and Se atoms in ridge positions on the edge facets as well. The attractive features of this model are that coordination to the sterically hindered, coordinatively saturated surface sites is not required and that the model is consistent with the experimental surface coverage determined by elemental analysis, {CdSe[n-octyl-amine]$_{0.53±0.06}$} (see Results).

The surface structure proposed here for the amine-passivated CdSe QBs resembles that calculated for CdSe nanosheets by Hyeon, Hoffmann, and co-workers.[28] Their surface structure features primary-amine ligands bound to Cd atoms in the ridge positions on the top and bottom facets but not to Cd atoms in the valley positions. Amine ligands bound to surface Se atoms are not present. That model, however, is inconsistent with our elemental analysis data, having too few amine ligands by half.

As reported in the Results, the overall composition of the Cd(oleate)$_2$-passivated QBs was determined to be {CdSe[Cd-(oleate)$_2$]$_{0.19±0.02}$}. Surface models in which one Cd(oleate)$_2$ unit is bound for each surface Se atom in a ridge position are consistent with this composition. We imagine coordination of

the Cd atom in the Cd(oleate)$_2$ units to ridge Se atoms in a bridging μ_2 fashion as shown in Figure 12c. The IR data confirm that the oleate ligands adopt bridging modes, of which several variations are possible. We note that the ridge Cd atoms are nominally three-coordinate, such that oleate bridging to those Cd atoms could relieve their steric unsaturation. Thus, Cd(oleate)$_2$ surface bonding in the proposed μ_2 mode allows the Z-type Cd, the ridge Cd, and the ridge Se atoms to become coordinatively saturated, avoids interactions with the saturated valley atoms, is consistent with the IR data, and corresponds to the measured composition of {CdSe[Cd(oleate)$_2$]$_{0.19}$}.

We suggest that the surface configurations for n-octylamine and Cd(oleate)$_2$ binding proposed here clarify the L- and Z-type surface interactions depicted only schematically in Scheme 1.

Contributions of Strain and Dimensional Changes to the Reversible Exciton Energy Shifts. As noted in the Introduction, changes in the pressure exerted by the surfaces of nanocrystals upon the cores and changes in the dimensions (in this case, effective thicknesses) of the nanocrystals may both contribute to changes in exciton energies. Here, we separate and analyze those contributions.

Table 4 records the strain states of the variously passivated 2D II–VI nanocrystals, determined by XRD. The nanocrystals are under varying degrees of compressive strain, with the strain being highest in the L-type, amine-passivated cases. The differences in strain ($\Delta\varepsilon$) and Young's modulus (Y) of the semiconductors determines the difference in surface pressure (or difference in stress, $\Delta\sigma$) exerted by the L- and Z-type surfaces. The expected spectral energy shifts (ΔE_{strain}) due to changes in the strain states are then determined from the band gap pressure coefficient (α) of the semiconductors. Overall, ΔE_{strain} is calculated by eq 1, which is derived in the Supporting Information.

$$\Delta E_{\text{strain}} = \alpha(\Delta\varepsilon)Y \tag{1}$$

Because the changes in strain are greater in lattice parameter a than in c (Table 4) and, more importantly, because only a has a component in the quantum-confined thickness dimension largely responsible for the reversible energy shifts, $\Delta\varepsilon$ was determined only from the varying strain in a. Additionally, because Young's modulus is not known precisely for CdSe or CdS, we calculated Y from the bulk modulus B and Poisson's ratio μ for these semiconductors. In these calculations, we employ bulk values for α, B, μ, and Y. The details are given in the Supporting Information. The energy shifts ΔE_{strain} so obtained are recorded in Table 5.

Table 5 compares the energy shifts observed spectroscopi-cally for the Z-type surface passivation, relative to the L-type, n-

octylamine-passivated nanocrystals, to the energy shifts (ΔE_{strain}) predicted by the observed changes in the strain states of the nanocrystals. Interestingly, the spectral shifts obtained by $Zn(\text{oleate})_2$ passivation agree quantitatively with the values calculated from the changes in strain. That is, the spectral shifts observed for $Zn(\text{oleate})_2$ passivation may be attributed entirely to strain differences ($\Delta\varepsilon$).

In contrast, $\Delta\varepsilon$ can account for only a portion of the spectral shifts observed for $Cd(\text{oleate})_2$ passivation of the CdSe and CdS nanocrystals (ΔE_{strain}; Table 5). The components unaccounted for by changes in strain states ($\Delta E_{\text{thickness}}$; Table 5) are of comparable magnitude to those predicted by $\Delta\varepsilon$, indicating that they are due to comparably large effects. We propose that these additional components in the spectral shifts for the $Cd(\text{oleate})_2$ cases are due to extension of the CdSe and CdS lattices by the Cd atoms in the coordinated $Cd(\text{oleate})_2$ units, providing an effective thickness increase.

Useful comparisons may be drawn by comparing the spectral shifts that occur from $Cd(\text{oleate})_2$ passivation to those occurring upon addition of complete II−VI monolayers to the 2D II−VI nanocrystals. As noted above, the CdSe QBs employed here contain five monolayers in the thickness dimension. Addition of a complete sixth CdSe monolayer to the QBs results in a shift of the lowest-energy absorption from 2.76 to 2.40 eV, or by 360 meV.[18] This corresponds to the addition of one Cd and one Se atom for each Cd and Se atom in, for example, the top monolayer of the five-monolayer QB.

Upon passivation of the CdSe QBs by $Cd(\text{oleate})_2$, the equivalent of one Cd atom (in/from the $Cd(\text{oleate})_2$) has been added for (not *to*) every ridge Cd atom on the top and bottom QB facets, corresponding to half of the Cd atoms from the CdSe lattice on these surfaces. No Se atoms have been added. Thus, we may imagine the surface coordination of $Cd(\text{oleate})_2$ as adding a quarter of a monolayer to the top facet and a quarter of a monolayer to the bottom facet, for a total of a half of a monolayer. A true half monolayer of CdSe should have caused a shift to lower energy of approximately 360/2 meV, or 180 meV. A half monolayer consisting entirely of Cd atoms is not electronically equivalent to a true half CdSe monolayer and has apparently induced a (nonstrain) shift component of 87 meV (Table 5), within an order of magnitude of that predicted for a true half monolayer and fairly close for such a crude approximation. We consider that the addition of $Cd(\text{oleate})_2$ to the QB surfaces allows the exciton wave functions to delocalize to the Cd atoms within this passivation layer and therefore to have effectively increased the confinement dimension, or the thickness of the box.

A similar analysis may be applied to the CdS QPs. The amine-passivated $\{CdS[n\text{-octylamine}]_p\}$ QPs used here have a thickness of four CdS monolayers.[18] Addition of a complete fifth CdS monolayer results in a shift of the lowest-energy absorption from 3.28 to 2.98 eV, or by 300 meV.[18,29] Addition of a half monolayer of CdS should have caused a shift to lower energy of approximately 300/2 meV, or 150 meV. Addition of a half monolayer of Cd atoms by passivation with $Cd(\text{oleate})_2$ has induced a shift component of 39 meV (Table 5), as above, within an order of magnitude of that expected of a true half CdS monolayer and fairly close for a crude approximation. Thus, the effective thickness dimension of the CdS QPs has been increased by exchanging L-type amine passivation for Z-type $Cd(\text{oleate})_2$ passivation.

Significantly, Z-type passivation with $Zn(\text{oleate})_2$ does not increase the effective thickness dimension of the CdSe or CdS nanocrystals; in those cases, the spectral shifts observed are due entirely to changes in the strain states (Table 5 and the discussion above). Thus, addition of Zn atoms to the top and bottom surfaces does not induce exciton delocalization into the $Zn(\text{oleate})_2$ passivation layers. Rather, the excitons remain confined within the CdSe and CdS lattices. Recall that the Zn atoms in $Zn(\text{oleate})_2$ are coordinating to surface Se and S atoms, respectively, forming nascent ZnSe and ZnS layers. The band offsets of ZnSe and ZnS relative to those of CdSe and CdS, respectively, indicate that these should be Type-I interfaces,[31,32] thus confining the electrons and holes within the CdSe and CdS core lattices.

The observations and argument presented here parallel those previously presented by Dubertret and co-workers for reactions of zinc-blende CdSe nanoplatelets.[33] They reported similar shifts in absorption features to lower energy upon exchange of carboxylate ligands by thiolate ligands and proposed that the shifts were due to relaxation of exciton confinement into the added thiolate passivation layers. They noted that the magnitudes of the shifts were comparable to those obtained by adding a complete CdSe monolayer.

◼ CONCLUSIONS

The large, reversible spectral shifts observed in 2D CdSe and CdS nanocrystals when L-type amine passivation is exchanged for Z-type $Cd(\text{oleate})_2$ passivation have both strain and confinement dimensionality components of comparable magnitude. Excitons delocalize into the $Cd(\text{oleate})_2$ passivation layers. In contrast, the smaller, reversible spectral shifts that occur upon exchanging amine and $Zn(\text{oleate})_2$ passivation are due only to strain, as the surface-bound Zn atoms do not extend the CdSe and CdS lattices. We propose that the fairly large changes in the strain states upon surface exchange are due to the very large surface areas of the 2D II−VI nanocrystals and that the large spectral shift components resulting from changes in confinement dimensionality are due to the small thicknesses of the nanocrystals.

◼ ASSOCIATED CONTENT

ⓈSupporting Information

The Supporting Information is available free of charge on the ACS Publications website at DOI: 10.1021/jacs.5b09343.

> NMR spectrum and relevant calculations, elemental analysis data and associated calculations of $\{CdSe[n\text{-octylamine}]_x\}$ and $\{CdSe[Cd(\text{oleate})_2]_y\}$, PL spectrum of purified $\{CdSe[Cd(\text{oleate})_2]_y\}$, HRTEM images of CdSe QBs before and after ligand exchange, TEM images of $\{CdS[n\text{-octylamine}]_p\}$ QPs, a derivation of eq 1, and calculation of Young's modulus for CdSe and CdS (PDF)

◼ AUTHOR INFORMATION

Corresponding Author

*buhro@wustl.edu

Notes

The authors declare no competing financial interest.

◼ ACKNOWLEDGMENTS

■ REFERENCES

(1) Anderson, N. C.; Hendricks, M. P.; Choi, J. J.; Owen, J. S. *J. Am. Chem. Soc.* **2013**, *135*, 18536.

(2) Munro, A. M.; Jen-La Plante, I.; Ng, M. S.; Ginger, D. S. *J. Phys. Chem. C* **2007**, *111*, 6220.

(3) Ji, X. H.; Copenhaver, D.; Sichmeller, C.; Peng, X. G. J. S. *J. Am. Chem. Soc.* **2008**, *130*, 5726.

(4) Munro, A. M.; Ginger, D. S. *Nano Lett.* **2008**, *8*, 2585.

(5) Frederick, M. T.; Amin, V. A.; Weiss, E. A. *J. Phys. Chem. Lett.* **2013**, *4*, 634.

(6) Koole, R.; Liljeroth, P.; de Mello Donega, C.; Vanmaekelbergh, D.; Meijerink, A. *J. Am. Chem. Soc.* **2006**, *128*, 10436.

(7) Koole, R.; Luigjes, B.; Tachiya, M.; Pool, R.; Vlugt, T. J. H.; de Mello Donega, C.; Meijerink, A.; Vanmaekelbergh, D. *J. Phys. Chem. C* **2007**, *111*, 11208.

(8) Buckley, J. J.; Couderc, E.; Greaney, M. J.; Munteanu, J.; Riche, C. T.; Bradforth, S. E.; Brutchey, R. L. *ACS Nano* **2014**, *8*, 2512.

(9) Haase, M.; Alivisatos, A. P. *J. Phys. Chem.* **1992**, *96*, 6756.

(10) Smith, A. M.; Mohs, A. M.; Nie, S. *Nat. Nanotechnol.* **2009**, *4*, 56.

(11) Simmonds, P. J.; Yerino, C. D.; Sun, M.; Liang, B. L.; Huffaker, D. L.; Dorogan, V. G.; Mazur, Y.; Salamo, G.; Lee, M. L. *ACS Nano* **2013**, *7*, 5017.

(12) Sadowski, T.; Ramprasad, R. *J. Phys. Chem. C* **2010**, *114*, 1773.

(13) Choi, C. L.; Koski, K. J.; Sivasankar, S.; Alivisatos, A. P. *Nano Lett.* **2009**, *9*, 3544.

(14) Li, J. B.; Wang, L. W. *Appl. Phys. Lett.* **2004**, *85*, 2929.

(15) Zhang, J. Y.; Wang, X. Y.; Xiao, M.; Qu, L.; Peng, X. *Appl. Phys. Lett.* **2002**, *81*, 2076.

(16) Wang, Y.; Herron, N. *Phys. Rev. B: Condens. Matter Mater. Phys.* **1990**, *42*, 7253.

(17) Meulenberg, R. W.; Jennings, T.; Strouse, G. F. *Phys. Rev. B: Condens. Matter Mater. Phys.* **2004**, *70*, 235311.

(18) Wang, F. D.; Wang, Y. Y.; Liu, Y. H.; Morrison, P. J.; Loomis, R. A.; Buhro, W. E. *Acc. Chem. Res.* **2015**, *48*, 13.

(19) Wang, Y. Y.; Zhou, Y.; Zhang, Y.; Buhro, W. E. *Inorg. Chem.* **2015**, *54*, 1165.

(20) Liu, Y. H.; Wang, F. D.; Wang, Y. Y.; Gibbons, P. C.; Buhro, W. E. *J. Am. Chem. Soc.* **2011**, *133*, 17005.

(21) Zelenak, V.; Vargova, Z.; Gyoryova, K. *Spectrochim. Acta, Part A* **2007**, *66*, 262.

(22) Morrison, P. J.; Loomis, R. A.; Buhro, W. E. *Chem. Mater.* **2014**, *26*, 5012.

(23) Li, Z.; Peng, X. G. *J. Am. Chem. Soc.* **2011**, *133*, 6578.

(24) Ithurria, S.; Tessier, M. D.; Mahler, B.; Lobo, R. P. S. M.; Dubertret, B.; Efros, A. *Nat. Mater.* **2011**, *10*, 936.

(25) Wang, Y. Y.; Zhang, Y.; Wang, F. D.; Giblin, D. E.; Hoy, J.; Rohrs, H. W.; Loomis, R. A.; Buhro, W. E. *Chem. Mater.* **2014**, *26*, 6318.

(26) Liu, Y. H.; Wayman, V. L.; Gibbons, P. C.; Loomis, R. A.; Buhro, W. E. *Nano Lett.* **2010**, *10*, 352.

(27) Joo, J.; Son, J. S.; Kwon, S. G.; Yu, J. H.; Hyeon, T. *J. Am. Chem. Soc.* **2006**, *128*, 5632.

(28) Son, J. S.; Wen, X. D.; Joo, J.; Chae, J.; Baek, S. I.; Park, K.; Kim, J. H.; An, K.; Yu, J. H.; Kwon, S. G.; Choi, S. H.; Wang, Z. W.; Kim, Y. W.; Kuk, Y.; Hoffmann, R.; Hyeon, T. *Angew. Chem., Int. Ed.* **2009**, *48*, 6861.

(29) Son, J. S.; Park, K.; Kwon, S. G.; Yang, J.; Choi, M. K.; Kim, J.; Yu, J. H.; Joo, J.; Hyeon, T. *Small* **2012**, *8*, 2394.

(30) Cooper, J. K.; Franco, A. M.; Gul, S.; Corrado, C.; Zhang, J. Z. *Langmuir* **2011**, *27*, 8486.

(31) Reiss, P.; Protiere, M.; Li, L. *Small* **2009**, *5*, 154.

(32) Wei, S. H.; Zunger, A. *Appl. Phys. Lett.* **1998**, *72*, 2011.

(33) Mahler, B.; Nadal, B.; Bouet, C.; Patriarche, G.; Dubertret, B. *J. Am. Chem. Soc.* **2012**, *134*, 18591.